Cement and Concrete Research xxx (xxxx) xxx–xxx

Contents lists available at ScienceDirect

Cement and Concrete Research

journal homepage: www.elsevier.com/locate/cemconres

Reactive transport modelling of a cement backfill for radioactive waste disposal

James C. Wilson[a,*], Steven Benbow[b], Richard Metcalfe[b]

[a] Quintessa Ltd., 633/635 Birchwood Boulevard, Warrington WA3 6QU, United Kingdom
[b] Quintessa Ltd., The Hub, 14 Station Road, Henley-on-Thames, Oxfordshire RG9 1AY, United Kingdom

ARTICLE INFO

Keywords:
Cement
Radioactive waste disposal
Reactive transport modelling

ABSTRACT

Cementitious materials are included in many geological disposal facilities for radioactive wastes, including the UK candidate backfill material Nirex Reference Vault Backfill (NRVB). As part of an ongoing programme of work to assess NRVB performance, 1-D reactive-transport models have been constructed to simulate reaction with different illustrative groundwater compositions. Variant cases were also produced to explore the effect of model assumptions on the predicted behaviour of the backfill. Depending on groundwater composition, cement alteration pathways included: carbonation; external sulphate attack; chloride attack; the formation of magnesium-rich solids; and the precipitation of secondary aluminosilicate minerals. In general, the models suggest that the pore space in backfill associated with radioactive waste disposal systems is likely to become clogged (to some degree) over time close to backfill-rock interfaces resulting in a reduction in capacity for solute transport. However, the models do not include all relevant process couplings which is potentially, an area for further work.

1. Introduction

Cementitious materials will be used as backfill, fracture grouts, and as matrices for waste encapsulation in many geological disposal facilities for radioactive wastes [1, 2]. The current candidate backfill material for use in a UK Geological Disposal Facility (GDF) in a Higher Strength Rock (HSR) is the Nirex Reference Vault Backfill (NRVB), which was developed in the 1990s [3]. NRVB comprises Ordinary Portland Cement (OPC) with a fine aggregate containing crushed limestone filler (primarily calcium carbonate) and hydrated lime (calcium hydroxide) [3]. The NRVB plays an important role in the multi-barrier approach of this disposal concept; one of the main safety functions of the NRVB is to provide a high-pH environment around waste packages, which limits both the corrosion of waste containers and the solubility of many radionuclides.

The properties and behaviour of NRVB have been the subject of research over many years and a significant body of understanding has been developed concerning both the chemical and physical properties of freshly cured samples, largely through laboratory experiments [3]. In terms of its performance to fulfil the desired key safety functions of a backfill in a GDF (namely maintaining high pH conditions to minimize waste container corrosion and radionuclide solubilities), the leaching characteristics have been studied [4]. More recent work has been focussed on the impact of ageing and alteration processes on the evolution of cement backfills, such as carbonation [5] and uptake of chloride [6]. However, less attention has been given to modelling NRVB behaviour using reactive-transport approaches. One previous study [7] that was part of a wider programme of work including that presented here, considered NRVB backfill in a 'vault scale' simulation. However, the work presented here is different to that study: the focus here is on the interface between backfill and host rock; a wider range of possible cement alteration pathways are considered (including chloride attack, sulphate attack characterised by thaumasite formation and the potential precipitation of secondary clay minerals); model assumptions and uncertainties are considered in a number of 'variant' simulations; and one of the groundwater compositions considered has a lower salinity.

Reactive transport models are often used to predict behaviour of engineered barrier materials over different spatial scales in radioactive waste disposal systems [7–17] as the timescales of interest for risk assessment purposes, are generally on the order of thousands to hundreds of thousands of years. It is clearly not possible to simulate such extreme time-scales under laboratory conditions, especially for relatively slow processes such as mineral dissolution-precipitations. Although techniques such as using high water to solid ratios, large surface area-to-volume ratios and elevated temperatures can be used to promote reactions, such approaches may introduce conditions that are less representative of the system of interest [18]. However, experimental data are valuable in that even when conditions are imposed to speed-up

* Corresponding author.
E-mail addresses: jameswilson@quintessa.org (J.C. Wilson), stevenbenbow@quintessa.org (S. Benbow), richardmetcalfe@quintessa.org (R. Metcalfe).

https://doi.org/10.1016/j.cemconres.2018.06.007
Received 1 November 2017; Received in revised form 15 May 2018; Accepted 13 June 2018

reactions, they provide an indication of possible cement alteration phenomena, and the potential for reactions observed in experiments to occur under repository conditions can be explored further in modelling studies. Ideally, when developing an understanding of a complex system, experimental and modelling studies should be complementary, with experimental and modelling studies being used to inform one another.

Other types of data that can be used to consider longevity of engineered barrier materials include natural and industrial analogues, and several examples have been identified for cementitious materials and cement-rock interaction [19, 20]. The pyro-metamorphic rocks and associated hyperalkaline groundwater plumes of the Maqarin site are of particular interest and have been investigated by various radioactive waste management agencies since 1989 [19, 21, 22]. These studies have the benefit that reactions have proceeded for long timescales (many human lifetimes to geological time scales). The potential drawbacks with analogue studies however, is finding sites where conditions are relevant to the engineered system of interest and ensuring correct interpretation of often highly-complex mineral assemblages that have evolved under changing conditions. That is not to say that reactive transport models are without problems, in that model development always entails a degree of simplification and the making of various assumptions, not to mention dealing with uncertainties in input data. Therefore multiple 'lines of evidence' are usually consulted to build a conceptual picture of the evolution of a radioactive waste disposal system, such that scenarios can be developed for radionuclide transport modelling and risk assessment calculations.

In recent years, work has been undertaken to produce reactive-transport models of industrial analogues of cement and cement-rock interaction (such as the Tournemire analogue, [20]) along with natural analogues such as Maqarin [21, 22] and saline alkaline lakes [23]. These studies suggest that the main long-term processes that are likely to operate in radioactive waste disposal systems can be simulated reasonably well, although there are some uncertainties associated with reaction kinetics (especially rates of mineral precipitation and growth) and thermodynamic data for minerals. However, the models provide some measure of confidence that typical modelling approaches can reasonably simulate long-term behaviour in 'real world' systems. Modelling studies have also been undertaken to simulate laboratory experiments of cement leaching [24, 25] and cement leaching in situ at underground laboratories [25, 26].

Previous 'blind' modelling studies of cement evolution in radioactive waste disposal facilities have been undertaken, especially focussing on the capacity of hyperalkaline cement porefluids to destabilise bentonite primary minerals and those present in claystone host rocks [e.g. 7, 8, 9, 10, 12, 13, 14]. In this study, reactive-transport simulations are presented that explore the potential for different modes of cement alteration to occur in NRVB, which is included as a component of the Engineered Barrier System in RWM's illustrative disposal concept for a GDF in a higher strength host rock. The simulations consider two illustrative water compositions of different ionic strengths, with different levels of salinity and different sulphate concentrations. Possible implications of cement alteration for porewater pH evolution and backfill performance are identified, and potential areas for further work are discussed.

2. Methods

2.1. Outline of approach

To develop detailed reactive-transport models of NRVB evolution, the following steps were undertaken:

(1) Development of the conceptual model, including definition of physical processes, geometry and discretization (Section 2.2)
(2) Selection of model input data (Section 3), based on literature review and supporting thermodynamic modelling, including: hydrated NRVB composition (Section 3.1); illustrative groundwater compositions (Section 3.2); potential cement alteration products (Section 3.3); thermodynamic data for hydrolysis reactions (Section 3.4); calculation of initial cement porewater composition and identification of aqueous species using thermodynamic modelling (Section 3.5); selection of kinetic data for primary and secondary solid dissolution/precipitation reactions (Section 3.6); selection of hydraulic and solute transport data (Section 3.7).
(3) Specification of model cases, including 'base cases' and 'variant cases' to explore implications of different model assumptions and uncertainties associated model input data (Section 3.8).
(4) Selection of modelling software considering physical and chemical processes and their couplings (Section 2.3)
(5) Construction of models and collation of model output data (Section 4).

2.2. Conceptual model development: physical processes and geometry

Cement backfill (NRVB) is included in the illustrative disposal concept for a UK GDF for Intermediate Level Waste (ILW) within 'higher-strength' rocks, through which groundwater flows via fractures. At present, work is ongoing in the UK to identify potential sites for a GDF. In the 2010 ILW disposal concept [27] the NRVB at the sides of the ILW vaults is ~1 m thick in both the shielded and unshielded concepts with an outer 0.2 m-thick layer of 'sprayed concrete'. At the base of the vaults, the NRVB is ~0.5 m thick.

Given that the objective of the work is to determine possible cement alteration behaviour for different illustrative geochemical conditions (rather than simulate specific vault geometries that will vary between disposal concepts suitable for different geological environments), 1-D models were constructed to simulate a block of cement (1 m thick) that is in contact with illustrative water compositions (Fig. 1). Depending on the distribution of fractures or faults in the rock, different surface areas of water-cement interfaces could be present. However, the simple model geometry was considered appropriate for identifying possible alteration behaviour and competing 'modes' of cement alteration.

It was assumed that the temperature is 25 °C throughout the simulations described herein, noting that there could be a short time-period

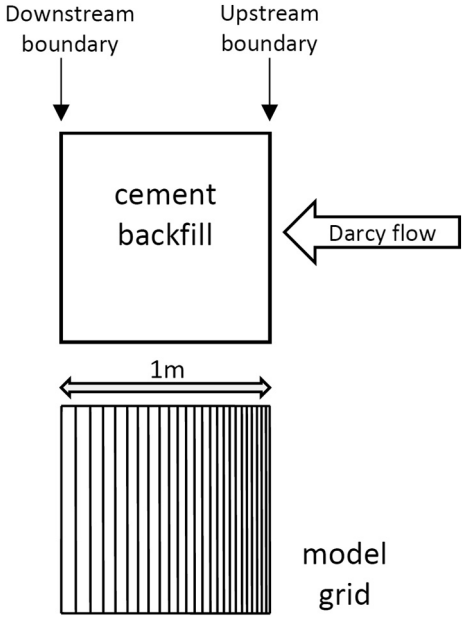

Fig. 1. Model geometry used in reactive transport simulations of NRVB-groundwater interaction. The cell widths were distributed geometrically; the smallest cell at the groundwater interface was 2 cm wide.

of relatively higher temperature conditions in the early post-closure phase of GDF evolution.

2.3. Conceptual model development: software

Fully-coupled 1-D reactive transport models were constructed using the Quintessa software 'MINARET' (MINeral Alteration due to REactive Transport [28]). MINARET was chosen for the modelling in preference to 'off-the-shelf' codes such as PHREEQC, as it allows full coupling of porosity evolution (as minerals dissolve and precipitate) with diffusive and advective transport. In addition, MINARET uses an adaptive time-stepper to maximise solver efficiency, by reducing time-step sizes in response to external events (e.g. time-dependent inputs) or 'emergent events' (e.g. at the onset of precipitation of new minerals or complete dissolution of pre-existing minerals) and increasing time-step sizes when the system is undergoing more 'smooth' periods of evolution. MINARET uses the 'QPAC' solver engine was developed under the 'TickIT' software certification programme [29] and the general approach taken by QPAC (and MINARET) have been used in a several reactive transport modelling studies [16, 17, 20, 22, 23, 30].

Supporting calculations (aqueous speciation) were undertaken using PHREEQC [31] to generate initial cement porewater compositions and to identify the key aqueous species to include in reactive transport models. In addition, simple mineral-fluid equilibration calculations were undertaken using PHREEQC to support the interpretation of the more complex reactive-transport simulations.

The MINARET simulations included cement solid/mineral dissolution-precipitation reactions (kinetic treatment), aqueous speciation, solute transport (diffusive and advective transport) and porosity evolution. The models are based on simple porous medium assumptions and do not consider the evolution of cement cracks. In addition, the models focus on cement alteration, rather than explicit representation of both cement and host rock evolution.

The reactive transport simulations include a kinetic treatment of mineral dissolution/precipitation reactions, using a routinely-applied Transition State Theory (TST)-based approach [32] represented by [33]:

$$\frac{dS}{dt} = A(S)(k_1(a_{H+})^{n_1} + k_2 + k_3(a_{H+})^{n_3} + k_4(f_{CO_2})^{n_4})\left(1 - \frac{Q}{K}\right) \quad (1)$$

where S is the quantity of a solid of interest (mol), t is time (s), $k_{1,\,2,\,3,\,4}$ are the rate constants (mol/m^2/s) for acid, neutral, base and carbonate mechanisms, $A(S)$ is the mineral reactive surface area (m^2) (which is a function of the mineral abundance), n is a dimensionless catalysis constant for acid (n_1), base (n_3) and carbonate-dependent rates (n_4), Q is the ion activity product for the solid of interest, a_{H^+} is the activity of the hydrogen ion, f_{CO_2} is the CO_2 fugacity, and K is the equilibrium constant for the mineral (apart from $A(S)$ and k, these parameters are dimensionless). The mineral reactive surface area is a function of the mineral abundance, its specific surface area, A_{sp} (m^2/g) and its molecular weight, W (g/mol), and is given by $A(S) = A_{sp}\,W\,S$.

In all model cases, diffusion was coupled to porosity using a linear implementation of Archie's Law, i.e.:

$$D_{eff} = D_{pore} \times \theta \quad (2)$$

where D_{eff} is the effective diffusion coefficient, D_{pore} is the diffusion coefficient and θ is porosity (−).

In one of the 'variant' simulations, porosity was coupled to permeability using a Kozeny-Carman relationship:

$$K = \left[K_{ref} \times \left[\frac{(1-\theta_{ref})^2}{(\theta_{ref})^3}\right] \times \left[\frac{(\theta)^3}{(1-\theta)^2}\right]\right] \quad (3)$$

where K is hydraulic conductivity (m/s), K_{ref} is the initial hydraulic conductivity at the initial reference porosity (θ_{ref}) and θ (−) is porosity. In most of the simulations, alteration was promoted by not coupling permeability to porosity, thereby maximising transport of solutes through parts of the cement where porosity reduction has occurred.

Table 1
Model NRVB Compositions [34] with 55% porosity. C-S-H gel is treated as an ideal solid-solution (SS) of 'jennite-like' and 'tobermorite-like' compositional end members [35].

Solid phase [formula]	Composition 'H'		Composition 'F'	
	wt%	vol%	wt%	vol%
Portlandite $[Ca(OH)_2]$	23.2	11.6	19.8	9.5
C-S-H	24.8	11.5	23.9	10.6
(Jennite-like SS end-member) $[(CaO)_{1.6666}\,(SiO_2)(H_2O)_{2.1}]$		(10.4)		(9.6)
(Tobermorite-like SS end-member) $[(CaO)_{0.8333}\,(SiO_2)(H_2O)_{1.3333}]$		(1.1)		(1.0)
Hydrogarnet $[Ca_3Al_2(OH)_{12}]$	10.0	4.5	–	–
Calcite $[CaCO_3]$	42.0	17.4	38.2	15.2
Monocarboaluminate $[Ca_4Al_2(CO_3)(OH)_{12}{\cdot}5H_2O]$	–	–	12.6	6.3
Ettringite $[Ca_6Al_2(OH)_{12}(SO_4)_3{\cdot}26\,H_2O]$	–	–	5.5	3.3
Total	100.0	45.0	100.0	45.0
Porosity	0.0	55.0	0.0	55.0

3. Input data

3.1. NRVB composition

NRVB comprises Ordinary Portland Cement (OPC) with a fine aggregate containing crushed limestone filler (primarily calcium carbonate) and hydrated lime (calcium hydroxide) [3]. The composition of NRVB after hydration has been considered [34], and two suggested hydrated solid phase assemblages have been included in the models herein (Table 1). 'Model H' assumes that hydration takes place at an elevated (but relatively short-lived) temperature (up to ~80 °C), resulting in hydrogarnet being present rather than monocarboaluminate, whereas the 'Model F' composition assumes that both monocarboaluminate and ettringite form in addition to Portlandite and C-S-H gel [34].

3.2. Groundwater compositions

Two illustrative groundwaters relevant to crystalline rock in the UK were included in the models described herein (Table 2) as they cover a range of chloride and sulphate concentrations. However, it is recognised that several other water compositions could have been chosen.

3.3. Potential cement alteration products

Potential cement alteration products included in the reactive transport models are listed in Table 3. It is expected that the cement backfill present in a GDF will undergo a degree of leaching and degradation due to interaction with groundwater. There are a number of potential modes of cement alteration including: carbonation, i.e. the formation of carbonate minerals [5, 38]; magnesium attack (resulting in brucite formation or formation of other magnesium-bearing solids, commonly associated with seawater-cement or seawater-brine interaction [39]; sulphate attack (with alteration to minerals such as ettringite, gypsum and thaumasite [38, 40–43] and chloride attack (resulting in the formation of minerals such as Friedel's salt or Kuzel's salt [44].

In addition to cement leaching, carbonation and sulphate/magnesium/chloride attack, the interaction of cement with rock forming minerals is likely to result in a zone of alteration forming at cement-rock

Table 2
Illustrative (crystalline host rock) ground water compositions 'S1' (RCF3 DET5, [36]) and 'S2' (BH9B SPFT3 [37]). Note that I concentrations are not available for S2 (value of 1E-20 mol/kg assumed in model).

	S1	S2
pH	7.22	6.80
Ionic strength (mol/kg)	0.48	0.005
Concentration (mol/kg)		
Na	3.70E-01	8.40E-04
K	4.40E-03	3.76E-05
Mg	5.70E-03	5.35E-04
Ca	2.90E-02	1.02E-03
Sr	2.00E-03	5.74E-06
Ba	1.30E-06	4.73E-07
Al	1.70E-06	1.61E-09
C (TIC)	1.00E-03	2.75E-03
Si	2.50E-04	1.87E-04
SO_4^{2-}	1.20E-02	4.17E-05
F	1.20E-04	5.26E-06
Cl	4.20E-01	4.09E-04
Br	3.20E-04	3.23E-07
I	1.00E-06	–

Table 3
Potential cement alteration products included in reactive-transport models.

Possible alteration products	Composition
Calcite (also a primary solid)	$CaCO_3$
Dolomite	$CaMg(CO_3)_2$
Hydrotalcite	$Mg_4Al_2(OH)_{12}CO_3{\cdot}3H_2O$
OH-Hydrotalcite	$Mg_4Al_2(OH)_{14}{\cdot}3H_2O$
Ettringite (also a primary solid)	$Ca_6Al_2(OH)_{12}(SO_4)_3{\cdot}26H_2O$
Thaumasite	$Ca_6Si_2(OH)_{12}(CO_3)_2(SO_4)_2{\cdot}24H_2O$
Gypsum	$CaSO_4{\cdot}2H_2O$
Friedel's salt	$Ca_4Al_2Cl_{1.95}(OH)_{12.05}{\cdot}4H_2O$
Kuzel's salt	$Ca_4Al_2Cl(SO_4)_{0.5}(OH)_{12}{\cdot}6H_2O$
Brucite	$Mg(OH)_2$
Analcime	$Na_{0.96}Al_{0.96}Si_{2.04}O_6{\cdot}H_2O$
Laumontite	$CaAl_2Si_4O_{12}{\cdot}4H_2O$
Gismondine	$Ca_2Al_4Si_4O_{16}{\cdot}9H_2O$
Ca-Clinoptilolite	$Ca_{3.36}Al_{6.72}Si_{29.28}O_{72}{\cdot}23.4H_2O$
Mesolite	$Na_{0.676}Ca_{0.657}Al_{1.99}Si_{3.01}O_{10}{\cdot}2.647H_2O$
Mordenite	$Ca_{0.2895}Na_{0.361}Al_{0.94}Si_{5.06}O_{12}{\cdot}3.468H_2O$
Phillipsite	$K_{2.8}Na_{3.2}Ca_{0.8}Al_{7.6}Si_{24.4}O_{64}{\cdot}24H_2O$
Illite	$K_{0.6}Mg_{0.25}Al_{1.8}Al_{0.5}Si_{3.5}O_{10}(OH)_2$
Sepiolite	$Mg_4Si_6O_{15}(OH)_2{\cdot}6H_2O$
Chalcedony	SiO_2
$SiO_{2(am)}$	SiO_2
Na-Saponite	$Na_{0.33}Mg_3Al_{0.33}Si_{3.67}O_{10}(OH)_2$
Ca-Saponite	$Ca_{0.165}Mg_3Al_{0.33}Si_{3.67}O_{10}(OH)_2$
K-Saponite	$K_{0.33}Mg_3Al_{0.33}Si_{3.67}O_{10}(OH)_2$
K-Feldspar	$KAlSi_3O_8$

or cement-clay interfaces that includes a number of aluminosilicate minerals and Calcium Aluminium-Silicate-Hydrate (C-A-S-H) phases [9, 19, 23, 45]. At the time the models were constructed, there was a lack of thermodynamic data for C-A-S-H gels, therefore only representative clays, zeolites/feldspathoids, K-feldspar, and poorly-crystalline silica polymorphs (amorphous silica and chalcedony) were included in the reactive transport simulations. The minerals chosen were considered representative, as there is a very wide range of compositions within the mineral groups of interest [46] and the reliance on estimated thermodynamic data for many zeolite compositions also results in a degree of uncertainty in which specific compositions are of most relevance [45, 47].

Although less commonly discussed in the literature than C-S-H gel, M-S-H (Magnesium Silicate-Hydrate) gel may form in magnesium-rich systems and it may be a candidate cement alteration product in environments with relatively higher dissolved magnesium concentrations. Experimental work also suggests that Magnesium-Silicate-Hydrate (M-S-H) could form due to interaction of cement with magnesium sulphate solutions [48]. Thermodynamic data are sparse for M-S-H gel, so sepiolite (a magnesium-rich clay mineral) was included as a proxy in the model, as spectroscopic analyses of the material suggests that M-S-H bonding environments are like those of magnesium-rich clay minerals [49].

3.4. Thermodynamic data

A number of thermnodynamic databases are available for modelling cement evolution [51–53]. The approach taken here was to use Geochemist's Workbench database 'thermo.com.v8.r6' to which equilibrium constants (log K values) for hydrolysis reactions for solid cement phases and representative zeolite minerals were added. The GWB database is based on the EQ3/6 database that was developed at Lawrence Livermore National Laboratory (LLNL), which contains a wide range of minerals, aqueous species and gases. Log K values for cement solids were calculated using standard molal thermodynamic data (Gibbs free energy of formation) from the dataset by Lothenbach and co-workers that is often referred to as 'cemdata' [35, 54] (Table 4). This dataset includes an ideal solid-solution representation of C-S-H gel, comprising 'jennite-like' and 'tobermorite–like' end members. A similar approach has been taken for modelling work undertaken to support the international LCS (Long-term Cement Studies) research project [22, 26, 30]. Data have also been added for representative zeolite compositions [46] calculated using Gibbs free energy of formation data produced using the approach of Arthur et al. [47]. The log K values calculated for both cement solids and zeolites used data for aqueous species taken from the SUPCTR96 'dprons96'database [55] which is consistent with the data used in the GWB database.

3.5. Initial cement porewater composition and aqueous speciation

Initial NRVB porewater compositions (Table 5) were generated by equilibrating primary solids with water containing dissolved Na, K, Cl, Mg, S and I at concentrations measured in NRVB porewater [57] using PHREEQC and the LLNL.dat database to which cement solids were added (the LLNL database is compatible with the GWB database 'thermo.com.v8.r6+' that was used for reactive transport modelling, as it includes equilibrium constants generated using the same standard molal thermodynamic data).

In addition to the 'basis' aqueous species present in the database used for mineral hydrolysis reactions, dominant secondary aqueous complexes were identified from speciation modelling of illustrative groundwater and NRVB porewater. The following species were identified and included in the reactive transport simulations: AlO_2^-, $NaAlO_{2(aq)}$, $HAlO_{2(aq)}$, $BaCl^+$, $BaCO_{3(aq)}$, $HBr_{(aq)}$, $CO_{2(aq)}$, CO_3^{2-}, $CaCO_{3(aq)}$, $CaSO_{4(aq)}$, $CaCl^+$, $CaHCO_3^+$, $CaCl_{2(aq)}$, $KOH_{(aq)}$, KSO_4^-, $KCl_{(aq)}$, KBr, $MgSO_{4(aq)}$, $MgCO_{3(aq)}$, $MgCl^+$, $MgHCO_3^+$, $NaCl_{(aq)}$, $NaOH_{(aq)}$, $NaSO_4^-$, $NaHCO_{3(aq)}$, $NaHSiO_{3(aq)}$, $SrSO_{4(aq)}$, $SrCl^+$, $SrCO_{3(aq)}$, $HSiO_3$, $H_2SiO_4^{2-}$.

The 'Helgeson B-dot' method (an extended Debye-Hückel approach) was used in preference to the Davies equation and other approaches for mean solute activity calculations as it has the capacity to accurately model activity-concentration relationships in solutions of relatively high ionic strengths, reportedly being reasonably accurate to an ionic strength of ~1 mol/kg, or even up to ~3 mol/kg for NaCl-dominated water compositions [50, 58].

3.6. Kinetic data for dissolution-precipitation reactions

The compilation by Palandri and Kharaka [33] was used as the primary source of kinetic data (k and n values) for silicate and carbonate minerals (Eq. (1)). Additional data required for other minerals were taken from the published peer-reviewed literature (Table 6). Approximate rates of dissolution reactions for cement solids were taken from Baur et al. [59]. Where data were unavailable for a specific k term

Table 4
Thermodynamic data added to the GWB database 'thermo.com.v8.r6+' used in reactive transport modelling.

Solid phase	Hydrolysis reaction	log K (25 °C, 1 bar)	Molar V of solid (cm^3/mol)	Data source for solid
Portlandite	$Ca(OH)_2 + 2\ H^+ = Ca^{2+} + 2\ H_2O$	22.800	33.06	[54]
C-S-H high Ca/Si (Jennite-like end member)	$(CaO)_{1.6666}\ (SiO_2)(H_2O)_{2.1} + 3.3332\ H^+ = 1.6666\ Ca^{2+} + SiO_2 + 3.7666\ H_2O$	29.301	78.40	[54]
C-S-H low Ca/Si (Tobermorite-like end member)	$(CaO)_{0.8333}\ (SiO_2)(H_2O)_{1.3333} + 1.6666\ H^+ = 0.8333\ Ca^{2+} + SiO_2 + 2.1666\ H_2O$	11.137	58.70	[54]
Hydrotalcite	$Mg_4Al_2(OH)_{12}CO_3{\cdot}3H_2O + 13\ H^+ = 4\ Mg^{2+} + 2\ Al^{3+} + 15\ H_2O + HCO_3^-$	62.316	220.00	[54]
Hydrotalcite-OH	$Mg_4Al_2(OH)_{14}{\cdot}3H_2O + 14\ H^+ = 4\ Mg^{2+} + 2\ Al^{3+} + 17\ H_2O$	75.108	220.20	[54]
Ettringite	$Ca_6Al_2(OH)_{12}(SO_4)_3{\cdot}26\ H_2O + 12\ H^+ = 6\ Ca^{2+} + 2\ Al^{3+} + 3\ SO_4^{2-} + 38\ H_2O$	58.225	707.03	[54]
Hydrogarnet	$Ca_3Al_2(OH)_{12} + 12\ H^+ = 3\ Ca^{2+} + 2\ Al^{3+} + 12\ H_2O$	82.288	150.00	[54]
Monocarboaluminate	$Ca_4Al_2(CO_3)(OH)_{12}{\cdot}5H_2O + 13\ H^+ = 4\ Ca^{2+} + 2\ Al^{3+} + HCO_3^- + 17\ H_2O$	81.986	262.00	[54]
Friedel's salt	$Ca_4Al_2Cl_{1.95}(OH)_{12.05}{\cdot}4\ H_2O + 12.05\ H^+ = 4\ Ca^{2+} + 16.05\ H_2O + 2\ Al^{3+} + 1.95\ Cl^-$	76.136	271.51	[44]
Kuzel's salt	$Ca_4Al_2Cl(SO_4)_{0.5}(OH)_{12}{\cdot}6\ H_2O + 12\ H^+ = 4\ Ca^{2+} + 18\ H_2O + 2\ Al^{3+} + Cl^- + 0.5\ SO_4^{2-}$	74.614	288.52	[44]
Thaumasite	$Ca_6Si_2(OH)_{12}(CO_3)_2(SO_4)_2{\cdot}24\ H_2O + 6\ H^+ = 6\ Ca^{2+} + 2\ SO_4^{2-} + 2\ HCO_3^- + 2\ SiO_{2(aq)} + 32\ H_2O$	18.876	663.00	[56]
Phillipsite	$K_{2.8}Na_{3.2}Ca_{0.8}Al_{7.6}Si_{24.4}O_{64}{\cdot}24H_2O + 30.4\ H^+ = 2.8\ K^+ + 3.2\ Na^+ + 0.8\ Ca^{2+} + 7.6\ Al^{3+} + 24.4\ SiO_{2(aq)} + 39.2\ H_2O$	6.659	1218.2	[47]
Ca-clinoptilolite	$Ca_{3.36}Al_{6.72}Si_{29.28}O_{72}{\cdot}23.4H_2O + 26.88\ H^+ = 3.36\ Ca^{2+} + 6.72Al^{3+} + 29.28SiO_{2(aq)} + 36.84\ H_2O$	-15.621	1264.1	[47]

Table 5
Initial model NRVB porewater compositions (solute concentrations in mol/kg). It was assumed that the initial concentration of Ba and Br (reported in illustrative groundwaters) was close to zero (set at 1E-20 mol/kg at start of the simulations).

	Model H composition	Model F composition
pH	12.47	12.47
Na	1.93E-04	1.93E-04
K	6.50E-04	6.50E-04
Mg	2.03E-06	2.03E-06
Ca	1.90E-02	1.88E-02
Sr	0.00E + 00	0.00E + 00
Ba	0.00E + 00	0.00E + 00
Al	4.08E-04	3.54E-05
C (TIC)	7.76E-06	7.76E-06
Si	1.09E-06	1.09E-06
SO_4^{2-}	2.13E-05	2.22E-05
Cl	3.05E-06	3.05E-06
I	8.12E-07	8.12E-07

in Eq. (1), the value of that term was set to 0. Therefore, the dissolution rate of a mineral under pH conditions for which published rate data do not exist, is approximated.

Where data were completely unavailable, an analogue approach was used, whereby values for the solid phase of interest were assumed to be similar to those measured for a similar solid. Reactive surface area data (Table 7) are either reported values or were calculated based on geometric assumptions (spherical grains of 1 or 0.25 μm diameter for minerals considered to be more crystalline or very poorly crystalline, respectively). (Note that, given the uncertainty associated with kinetic data, a variant case was produced in which surface areas for all solids set to 1 m^2/g, all far-from-equilibrium mineral dissolution set at 1×10^{-5} mol/m^2/s.

3.7. Transport data

Transport data for NRVB are given in Table 8. For the simulations with HSR water compositions and the simulation that considers cement-NaCl interactions, advective flow was included (a list of model cases is provided in Table 9). In the base case simulations, the 'unleached' NRVB hydraulic conductivity of 1×10^{-9} m/s was used with a deterministic flow rate value from the 2010 NDA generic Disposal System Safety Case (DSSC) calculations (background Darcy velocity $q = 6 \times 10^{-4}$ m/y for vault backfilled with NRVB, giving a head gradient of 1.9×10^{-2} (−) [62]). A variant case considered the effect of cracking of the cement. In that case, the Darcy velocity was multiplied by a flow-focussing factor of 31.3 and hydraulic conductivity of 1.4×10^{-8} m/s was used (head gradient of 5.95×10^{-2}) to be consistent with the DSSC.

3.8. Specification of model cases

Several model cases were developed in which NRVB compositions (Table 1) were reacted with two illustrative groundwater compositions (Table 2). The maximum simulation time was set at 100000 years. The 'Model H' NRVB composition was used in most of the modelling (the 'base cases') with a variant case being produced using the alternative 'Model F' NRVB composition (Table 9). Variant cases were developed to explore different model assumptions on cement alteration, especially the assumptions made surrounding solute transport, such as the effect of coupling permeability to porosity (in the base case permeability was decoupled to encourage alteration, and thereby potentially provide a more cautious estimate of the extent of alteration). Given the uncertainties associated with kinetic input data, a case was also produced in which reactive surface area values and dissolution/precipitation rates were modified to arbitrarily chosen surface area values and far-from-equilibrium dissolution rates of 1 $^-m^2$/g and 1×10^{-5} mol/m^2/s, respectively. A variant case was also produced in which solute transport was decoupled from porosity evolution and mineral precipitation could occur even after the total volume of solids in the compartment was equal to the total compartment volume, i.e. no pore space was left. The complete lack of 'pore clogging' is not realistic and would not be expected. However, this approach provides some indication of how alteration pathways may continue to evolve if solutes are still able to penetrate partially-altered NRVB even after some pores become clogged due to temporal and spatial variability in cracking, for example.

Table 6
Rate data for mineral dissolution-precipitation (terms defined in Eq. (1)). Data for illite and saponite were produced by refitting reported experimental data.

Solid	Acid		Neutral	Base		Carbonate		Assumption/reference
	log k_1	n_1	log k_2	log k_3	n_3	log k_4	n_4	
	mol/m^2/s	–	mol/m^2/s	mol/m^2/s	–	mol/m^2/s	–	
Portlandite	–	–	−12.00	–	–	–	–	Ettringite analogue
C-S-H gel	–	–	−12.00	–	–	–	–	[59]
Calcite	−0.30	1.00	−5.81	–	–	−3.48	1.00	[33]
Hydrogarnet	–	–	−12.00	–	–	–	–	Ettringite analogue
Hydrotalcite	–	–	−12.00	–	–	–	–	Ettringite analogue
Hydrotalcite-OH	–	–	−12.00	–	–	–	–	Ettringite analogue
Ettringite	–	–	−12.00	–	–	–	–	[59]
Monocarboaluminate	–	–	−12.00	–	–	–	–	Ettringite analogue
Thaumasite	–	–	−12.00	–	–	–	–	Ettringite analogue
Gypsum	–	–	−2.79	–	–	–	–	[33]
Friedel's salt	–	–	−12.00	–	–	–	–	Ettringite analogue
Kuzel's salt	–	–	−12.00	–	–	–	–	Ettringite analogue
Brucite	−4.73	0.50	−8.24	–	–	–	–	[33]
Dolomite	−3.19	0.50	−7.53	–	–	−5.11	0.50	[33]
Analcime	–	–	−11.40	−13.9	−0.36	–	–	[9]
Laumontite	–	–	−11.40	−13.9	−0.36	–	–	Analcime analogue
Gismondine	–	–	−11.40	−13.9	−0.36	–	–	Analcime analogue
Ca-Clinoptilolite	–	–	−13.80	−16.34	−0.36			[60]
Mesolite	–	–	−13.80	−16.34	−0.36	–	–	Clinoptilolite analogue
Mordenite	–	–	−13.80	−16.34	−0.36	–	–	Clinoptilolite analogue
Phillipsite	–	–	−13.80	−16.34	−0.36			Clinoptilolite analogue
Illite	−11.78	0.56	−15.00	−20.07	−0.55	–	–	[17]
Sepiolite	−5.70	0.80	−12.40	–	–	–	–	Lizardite analogue [33]
Chalcedony	–	–	−12.77	–	–	–	–	[33]
$SiO_{2(am)}$	–	–	−12.77	–	–	–	–	[33]
Saponite-Na/Ca/K	−12.37	0.35	−14.54	−15.66	−0.18	–	–	Montmorillonite analogue [16]
K-Feldspar	−10.06	0.50	−12.41	−21.20	0.82			[33]

Table 7
Surface area data (A_{sp} term in Eq. (1)).

Solid	A_{sp} (m^2/g)	Assumption/reference
Portlandite	11.80	0.25 μm diameter spheres
C-S-H gel	41.00	BET data [59]
Calcite (also a secondary phase)	2.21	1 μm spheres
Hydrogarnet	9.49	0.25 μm diameter spheres
Hydrotalcite	11.94	0.25 μm diameter spheres
Hydrotalcite-OH	11.94	0.25 μm diameter spheres
Ettringite	9.80	BET data [59]
Thaumasite	9.80	Ettringite analogue
Monocarboaluminate	9.80	Ettringite analogue
Gypsum	10.40	0.25 μm diameter spheres
Friedel's salt	9.80	Ettringite analogue
Kuzel's salt	9.80	Ettringite analogue
Brucite	10.00	0.25 μm diameter spheres
Dolomite	2.11	1 μm diameter spheres
Analcime	0.25	BET measurement [61]
Laumontite	0.25	Analcime analogue
Gismondine	0.25	Analcime analogue
Ca-Clinoptilolite	10.10	75–150 μm size fraction [60]
Mesolite	10.10	Ca-Clinoptilolite analogue
Mordenite	10.10	Ca-Clinoptilolite analogue
Phillipsite	10.10	Ca-Clinoptilolite analogue
Illite	130.00	Rate normalised to BET total surface area [17]
Sepiolite	12.00	0.25 μm diameter spheres
Chalcedony	9.23	0.25 μm diameter spheres
$SiO_{2(am)}$	9.23	0.25 μm diameter spheres
Saponite-Na, Ca, K	111.00	BET total surface area, montmorillonite analogue [17]
K-Feldspar	2.31	1 μm spheres

Table 8
NRVB transport data used in reactive transport simulations.

Property	Value	Assumption/references
Porosity (−) (θ_{ref}) (initial)	0.55	[63]
D_{eff} (initial) (m^2/s) (upper value)	4.80E-10	[63]
D_{pore} (initial) (m^2/s) (upper value)	8.73E-10	($D_{pore} = D_{eff}/\theta_{ref}$)
Hydraulic Cond. K_{ref} (m/s)	1.00E-09	[64]
Hydraulic Cond. K_{ref} (m/s) (cracked)	1.40E-08	Unleached value × 10
Head gradient (m/m)	1.90E-02	See text.
Head gradient (m/m)(cracked)	5.95E-02	See text.

4. Results

4.1. Overview of results

The different simulations listed in Table 9 produced a large amount of output data, which cannot all be described in detail herein. Therefore, a summary of the main features of each model is given in Table 10. The table shows that the different water compositions resulted in different alteration characteristics, notably, the higher ionic strength 'S1' groundwater composition (ionic strength of 0.48 mol/kg) resulted in a significant amount of NRVB alteration to sulphate-rich and chloride-rich solids, along with some brucite ($Mg(OH)_2$) forming and pore clogging being relatively rapid (complete clogging at the cement-groundwater interface by 78 years). In contrast, the lower ionic strength 'S2' groundwater (ionic strength of 0.005 mol/kg) led to leaching and the precipitation of calcite ($CaCO_3$), along with saponite (an Mg-rich clay), and minor amounts of ettringite, with pore clogging taking 531 years.

Table 9
Summary of reactive transport simulation cases.

Identifier	Description
S1 base case	NRVB reacting with illustrative S1 water composition
S2 base case	NRVB reacting with illustrative 'dilute' S2 water
S1 variant 'F composition'	As base case, but using NRVB 'Model F' composition
S1 variant 'cracked'	Elevated diffusion coefficient and head gradient applied (Table 8 'cracked' values)
S1 variant 'permeability coupled'	Permeability coupled to porosity
S1 variant 'alternative kinetics'	Surface areas for all solids set to 1 m^2/g, all far-from-equilibrium mineral dissolution set at 1×10^{-5} $mol/m^2/s$
S1 variant 'no clog'	Volumes of cement solids/minerals decoupled from transport and total allowed to exceed 100 vol% (i.e. no pore clogging)

4.2. Base case results

In the S1 'base case', the alteration was characterised by a front of chloride attack, followed by a front of sulphate attack moving through the cement, resulting in the partial dissolution of primary portlandite, hydrogarnet and C-S-H gel. After only 5 years reaction time, Friedel's salt precipitation had occurred in the NRVB to a depth of ~40 cm from the upstream boundary, with thaumasite and ettringite precipitating nearer to the groundwater inflow boundary (Fig. 2). Relatively smaller amounts of brucite and OH-hydrotalcite also precipitated by this time.

As the simulation continued, the front of chloride attack moved deeper into the NRVB, with hydrogarnet becoming replaced by Friedel's salt (~50 cm from the inflowing groundwater boundary after 10 years). There was also the continued alteration of primary cement phases (mainly C-S-H gel) to thaumasite and ettringite in a narrower zone of alteration nearer to the cement-groundwater interface, with ettringite forming deeper into the cement. By 50 years, Friedel's salt penetrated the cement to a depth of ~80 cm from the inflow boundary (Fig. 2) and the porosity of the cement cell next to the boundary had almost been completely lost due to the precipitation of thaumasite, ettringite, and a smaller amount of brucite (the hydrotalcite produced earlier in the simulation dissolved). The cement porewater pH was ~13.3 throughout the cement by 50 years, except for the regions characterised by sulphate attack, where there was a sharp decrease to ~12.7 next to the groundwater inflow boundary (not shown). By 78 years, the pore space of the (2 cm thick) NRVB cell next to the groundwater inflow boundary was filled by cement alteration products and the simulation could not proceed further. The cement porewater pH remained elevated at ~13.3 throughout most of the cement, with a value of 12.4 occurring in the cell in contact with the groundwater boundary condition.

The S2 base case was characterised by initial partial dissolution of the portlandite, hydrogarnet and C-S-H gel near the groundwater inflow boundary, followed by a decrease in the Ca/Si ratio of the C-S-H gel (reflected by the relative proportion of 'tobermorite-like' compositional end-member increasing) as calcite precipitated along with smaller amounts of gismondine (a silica-poor zeolite mineral), along with OH-hydrotalcite followed by Ca-saponite (an Mg-rich swelling clay). By 50 years, alteration had occurred mainly in the first model cell with an increase in porosity occurring deeper in the cement. By 50 years there had been the complete loss of C-S-H gel occurring in the model cell next to the groundwater inflow boundary as calcite and relatively smaller volumes of gismondine, OH-hydrotalcite and Ca-saponite precipitated (resulting in a reduction in pore space from 55 to 36%). The volumes of alteration products (mainly gismondine) in the second, third and fourth cells from the groundwater inflow boundary that precipitated by 50 years were relatively small compared with the volumes of primary solids dissolved, leading to a significant increase in cement porosity from 55 to 70.9 vol% in the second cement cell. The cement porewater pH in the zone of alteration was ~11.5 after 50 years. Carbonation and the precipitation of calcite continued after 200 years, and there were small increases in the volumes of other alteration products and an overall increase in porosity upstream, mainly within ~20 cm of the groundwater inflow boundary. The simulation ran until 531 years, by which time the porosity of the model cell next the groundwater inflow boundary had decreased to zero, as calcite continued to precipitate. Interestingly, there was the dissolution of newly-formed gismondine alteration product in the second cell from the upstream boundary by this time. Dissolution of Portlandite continued between 200 and 531 years, with losses being within ~20 cm of the groundwater inflow boundary.

The porewater pH in the alteration zone tended to decrease during earlier times of the S2 simulation, with values decreasing with distance from 12.4 to 11.8 in the 20 cm-thick alteration zone by 100 years. However, as the porosity of the cement decreased at the interface with the groundwater inflow boundary, pH recovered in the alteration zone to a value of ~12, which appears to have destabilised the gismondine which had formed as an alteration product.

4.3. Variant case results

Two variant cases were produced to explore the effects of assumptions made on solute transport on predicted cement evolution. In the S1 'cracked' variant, the elevated hydraulic conductivity (10 times higher than that measured on fresh NRVB) resulted in alteration proceeding more rapidly than in the base case as reactants were transported more rapidly into the cement and pore clogging occurred after 30 years (rather than 78 years) with alteration of hydrogarnet to Friedel's salt occurring ~10 cm deeper into the cement (not shown). In the 'permeability' variant, the inclusion of porosity-permeability coupling led to a decrease in the rate of solute transport through the cement, with pore clogging not occurring until 130 years, but with the nature and extent of alteration being indistinguishable compared with that produced in the base case simulation by 78 years.

There is significant uncertainty associated with assumptions made

Table 10
Summary of reactive transport model results.

Model identifier	Alteration products (*italics if also primary present as primary solid*)	Time to clogging (years)
S1 base case	Friedel's salt, ettringite, thaumasite, brucite	78
S2 base case	*Calcite*, Ca-saponite, OH-hydrotalcite, minor ettringite (gismondine, transient)	531
S1 variant 'cracked'	Friedel's salt, ettringite, thaumasite, brucite	30
S1 variant 'permeability'	Friedel's salt, ettringite, thaumasite, brucite	130
S1 variant 'alternative kinetics'	Friedel's salt, ettringite, thaumasite, brucite	110
S1 variant 'F composition'	Friedel's salt, *ettringite*, thaumasite, brucite, OH-hydrotalcite	91
S1 variant 'no clog'	Friedel's salt, ettringite, thaumasite, brucite, Na-saponite, calcite, mesolite, sepiolite, K-feldspar, chalcedony	(No clogging)

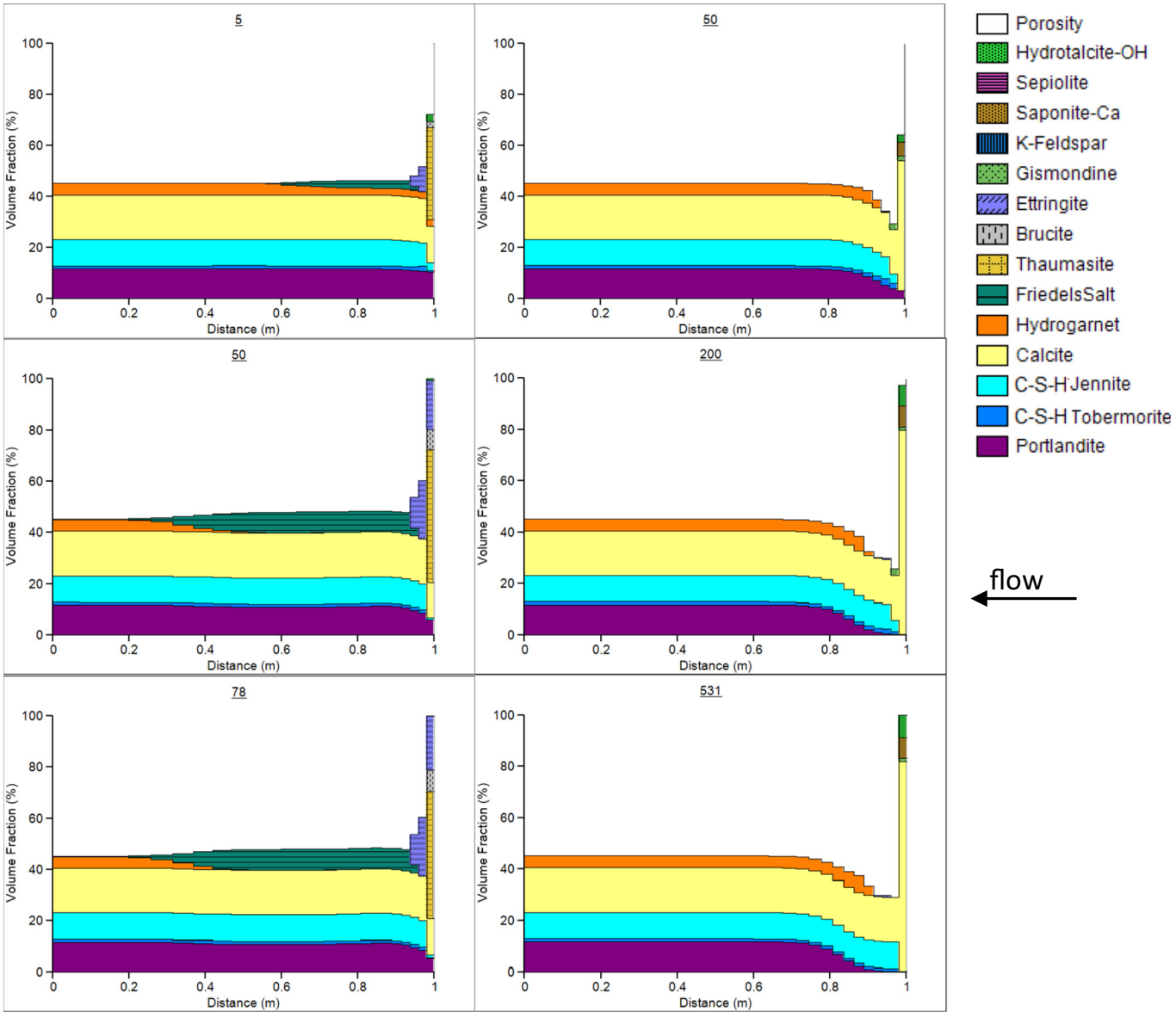

Fig. 2. Volume fraction plots for S1 (left) and S2 (right) base case simulations at key simulation output times. The values on the x-axis are distance from the groundwater outflow boundary (Fig.1), i.e. the "inner" side of the NRVB (flow is right to left).

on reactive surface areas and the use of analogues for mineral dissolution rates under far-from-equilibrium conditions. There is also significant uncertainty associated with using the same rate equation for both dissolution and precipitation reactions. In the 'alternative kinetics' variant case, the same reactive surface area and a 'rapid' rate was applied to all solids. This approach resulted in the more rapid movement of the chloride-attack front through the cement in the variant case, with all hydrogarnet having been lost by 78 years. However, the overall mode of alteration and the thickness of the sulphate/magnesium alteration zone were similar in the variant case compared with the base case, but there was more extensive loss of portlandite in the two cement cells next to the groundwater inflow boundary in the variant case and a small amount of porosity remained in the cell next to the groundwater inflow boundary (0.8%).

In the 'no clogging' simulation, pore clogging was deactivated, such that the cells in the model could have a total volume that exceeded 100%. Although this approach is unrealistic, it does provide some indication of potential later-stage cement alteration pathways that may result if transport continues through backfill as it is leached (due to ongoing crack formation or 'armouring' of surfaces acting to keep larger fractures open, for example). The evolution of this case was the same as the base case until pore clogging of the upstream part of the cement at 78 years, after which time the alteration front dominated by products of sulphate attack continued to move deeper into the cement, penetrating the cement to a depth of 45 cm from the groundwater inflow boundary by 1000 years (Fig. 3). A second alteration front had also advanced into the cement by 1000 years that was dominated by products of magnesium attack, notably brucite, Na-saponite and OH-hydrotalcite, with a third front moving into the cement dominated by carbonation. By 1000 years the cement porewater pH closer to the inside of the cement was 12.4, having decreased from 13.3 at 78 years. The porewater pH at 1000 years decreased through the zone of sulphate attack and magnesium attack, with a minimum value of 7.5 occurring in the cement cell in contact with the groundwater inflow boundary. Between 1000 and 10,000 years, the alteration fronts moved deeper into the NRVB, with the sulphate-attack front having penetrated the entire model cross section by 5000 years and the zone characterised by Mg-rich minerals reached a depth of ~25 cm from the groundwater inflow boundary.

Between 1000 and 2000 years, the alteration fronts continued to penetrate the cement, with the front of sulphate attack having extended

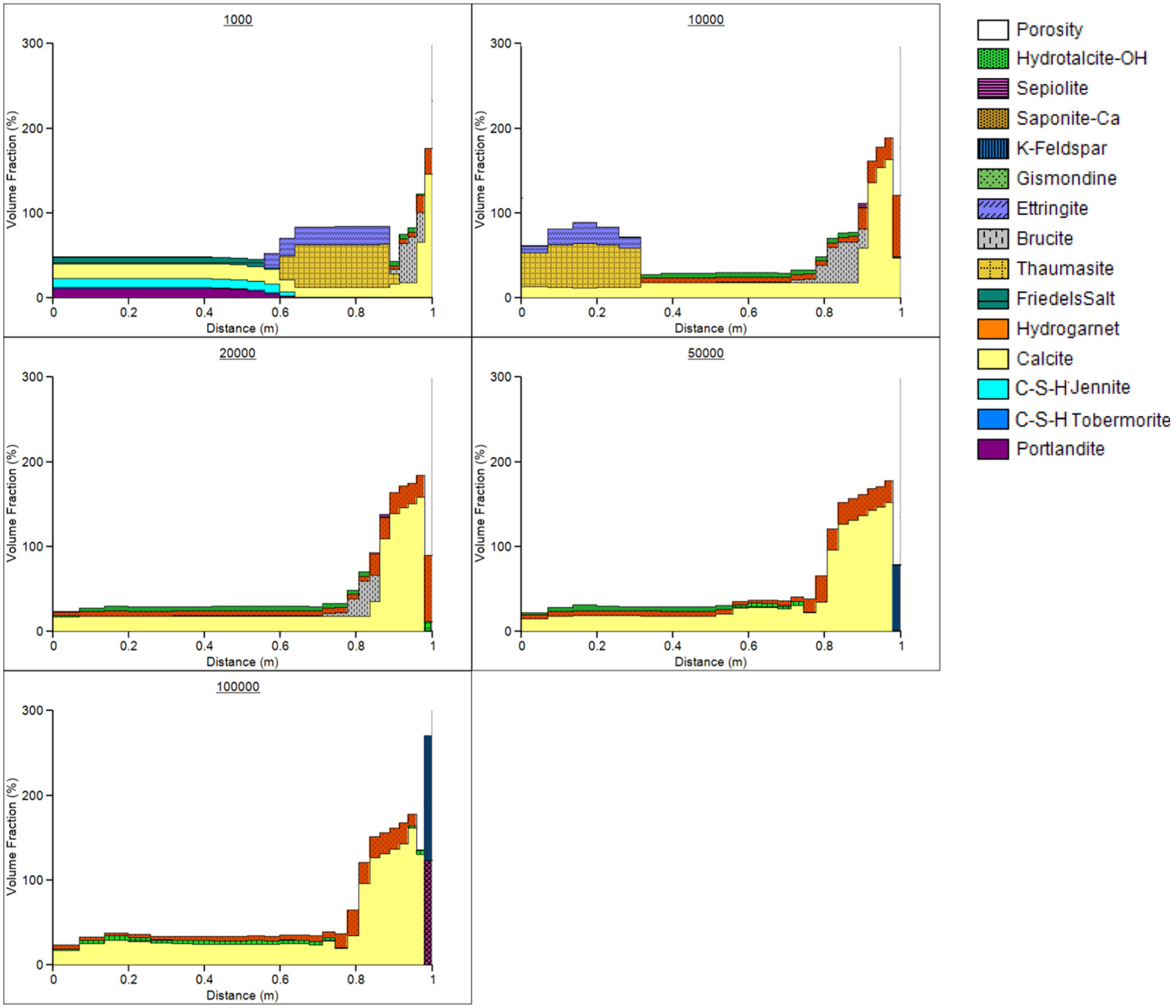

Fig. 3. Volume fraction plots for S1 'no clogging' variant case at key output times (years).

~65 cm into the cement from the groundwater inflow boundary. The magnesium-attack front reached a depth of ~16 cm by 2000 years, with carbonation occurring to a depth of ~4 cm from the groundwater boundary. By 5000 years, the sulphate-attack front had penetrated the entire model cross section, with only small amounts of portlandite and C-S-H gel remaining towards the groundwater outflow boundary. The zone of carbonation now extended to a depth of ~8 cm from the groundwater inflow boundary with mineral volumes approaching 200% of the actual volume of the cement. The cement porewater pH by 5000 years was 12 in the 20 cm wide region next to the groundwater outflow boundary where primary cement solids remained, with values gradually decreasing with depth towards the groundwater inflow boundary to a value of ~10. The pH in the cement cell next to the groundwater boundary was 7.3 by 5000 years.

By 10,000 years, only calcite remained as a primary solid; ettringite and thaumasite alteration products had largely dissolved out of the middle third of the cement cross section and been replaced by relatively smaller volumes of Na-saponite and OH-hydrotalcite (Fig. 3). The zone of brucite precipitation did not increase in width but there was the precipitation of a small amount of sepiolite next to the zone dominated by carbonation. By 10,000 years, the cement porewater pH was ~10.6 towards the groundwater outflow boundary region where thaumasite and ettringite remained, whereas in the middle part of the cement (where calcite, Na-saponite and OH-hydrotalcite were the main solids), the pH was ~9.6. There was a sharp decrease in pH from the middle part of the carbonation zone towards the groundwater inflow boundary, where the pH was 7.3.

Between 10,000 and 20,000 years, thaumasite and ettringite dissolved out of the cement leaving calcite, Na-saponite, OH-hydrotalcite and a very small amount of mesolite being present in a zone extending ~30 cm from the groundwater outflow boundary, with a porosity of ~70% (Fig. 3). The 30 cm wide zone in contact with the groundwater inflow boundary largely comprised secondary calcite, brucite and Na-saponite. In the cell next to the groundwater inflow boundary, calcite had been lost by 20,000 years, and the alteration products consisted of Na-saponite and mesolite. The pH of the cement porewater had decreased by 20,000 years, with a value of 8.7 at the groundwater outflow boundary, increasing to ~9.5 in the middle third of the cement cross-section, with a decrease through the carbonated zone to reach a minimum value of 7.3 in the cell next to the groundwater inflow boundary (Fig. 3).

Between 20,000 and 50,000 years, brucite dissolved out of the cement and the OH-hydrotalcite present in carbonation zone towards the

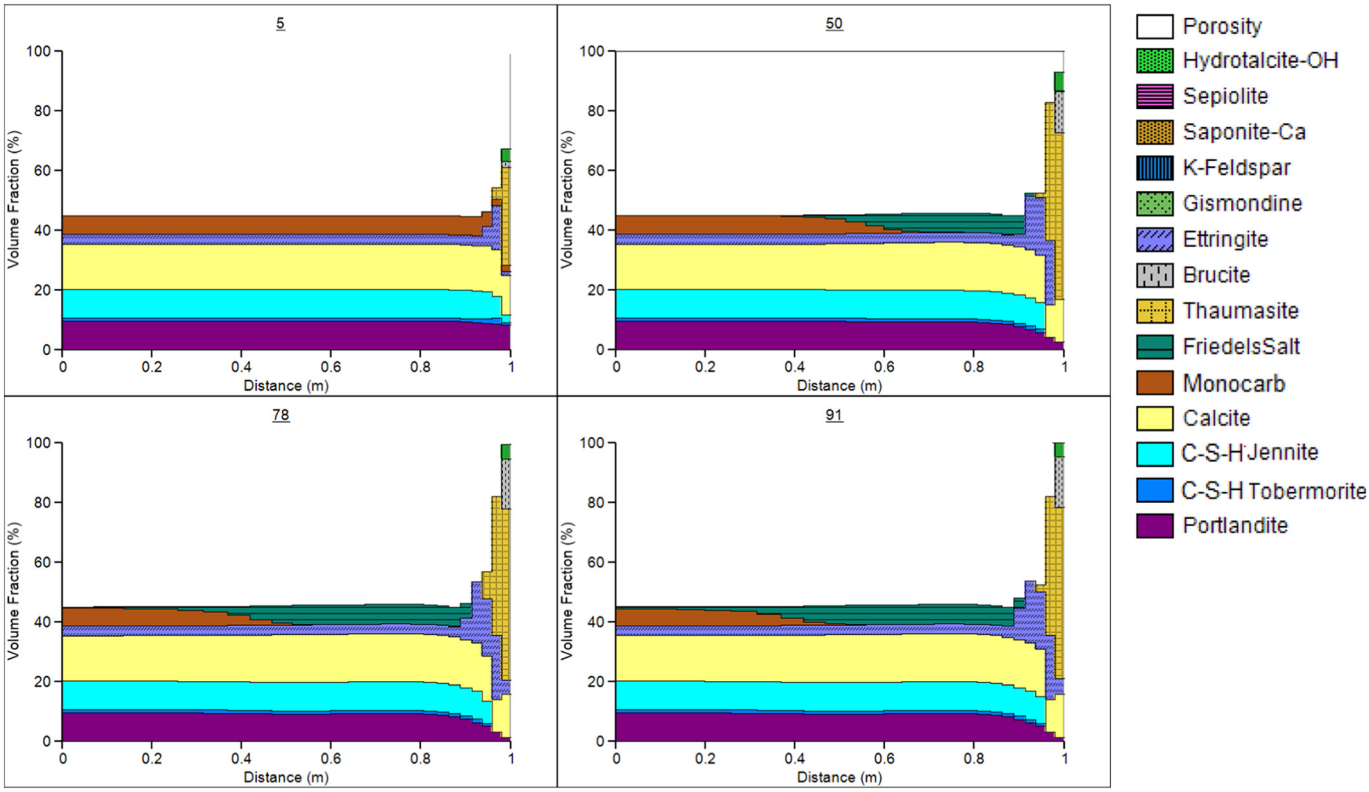

Fig. 4. Volume fraction plots for S1 'F composition' variant case at key output times (years).

groundwater outflow boundary was dissolved and replaced by mesolite by 50,000 years (Fig. 3). In addition, by 50,000 years, the Na-saponite and mesolite present in the cement cell at the cement-groundwater interface was replaced by K-feldspar. By 50,000 years the cement porewater pH ranged from ~8.6 at the groundwater outflow boundary to ~45 cm from the groundwater inflow boundary, with values falling throughout the zone of carbonation, reaching a minimum value of 7.3 in the cell in contact with the groundwater inflow boundary.

Between 50,000 and 100,000 years a front of alteration in which OH-hydrotalcite was replaced by mesolite moved through the cement away from the groundwater inflow boundary, such that by 100,000 years, all of the OH-hydrotalcite had been replaced (Fig. 3). In the cement cell next to the groundwater inflow boundary, there was the ongoing precipitation of K-feldspar and there was also the precipitation of chalcedony, mainly between 80,000 and 100,000 years. The porewater pH was ~7.3 throughout the 1-D model cross-section by 100,000 years.

In the S1 'F composition' variant case, NRVB alteration was broadly similar to that in the base case simulation, but with monocarboaluminate rather than hydrogarnet being replaced by Friedel's salt (Fig. 4) and pore clogging not being complete until 91 years. Alteration also resulted in the formation of ettringite as it did in the base case, thereby adding to that present as a primary solid. Thaumasite also formed as a product of sulphate attack, as in the base case; brucite also precipitated as an alteration product at the upstream boundary. In the variant case, the thickness of the sulphate-rich alteration zone is a little greater than that in the base case with alteration extending ~20 cm into the cement, whereas in the base case it was ~8 cm by 78 years.

5. Discussion

5.1. Cement alteration pathways

The main objective of this study was to determine possible cement alteration pathways that may occur due to NRVB reacting with groundwater in crystalline rock. Reaction with the 'S1' groundwater composition (ionic strength of 0.48 mol/kg; dissolved sulphate concentration of 1.2×10^{-2} mol/kg) led to significant sulphate attack, with the formation of ettringite and thaumasite alteration products (thaumasite having been excluded in previous work [7]). Friedel's salt also formed, and in order to understand the concentration of Cl^- required for this to occur, a simple PHREEQC calculation was undertaken whereby the S1 water was equilibrated with portlandite, hydrogarnet and Friedel's salt at 25 °C, 1 bar. The resulting model pH is 12.45, and the calculated chloride concentration is 4.95×10^{-3} mol/kg. Therefore, groundwater that has a dissolved total Cl concentration significantly greater than $\sim 5 \times 10^{-3}$ mol/kg may tend to promote Friedel's salt precipitation in the presence of aluminous cement solids such as hydrogarnet, assuming sufficient masses of reactants for the reaction are available and crystal growth is not kinetically inhibited. For more dilute groundwater compositions that have a lower chloride content, such as illustrative S2 groundwater, chloride attack appears to be a less likely type of cement alteration.

The different modes of cement alteration have different implications for porewater pH evolution. The alteration of hydrogarnet to Friedel's salt resulting in a pH increase to ~13 in Portland cement has been reported elsewhere [65] and a simplified reaction can be written:

$$Ca(OH)_{2(s)}(\text{portlandite}) + 3CaO{\cdot}Al_2O_3{\cdot}6H_2O_{(s)}(\text{hydrogarnet}) + 2Cl^- + 4H_2O \rightarrow 3CaO{\cdot}Al_2O_3{\cdot}CaCl_2{\cdot}10H_2O_{(s)}(\text{Friedel's salt}) + 2OH^-$$

In systems where there is magnesium attack, backfill porewater pH may tend to evolve towards a value of ~10, which is associated with brucite ($Mg(OH)_2$) equilibrium, whereas the presence of magnesium silicates such as sepiolite (used as an analogue for M-S-H) may result in lower pH conditions. For example, sepiolite equilibrated with pure water at 25 °C, 1 bar (using PHREEQC) results in a pH of 9.6.

Carbonation tends to result in a pH of ~7 to 8, depending on pCO_2 and the composition of the groundwater (noting that calcite equilibrium in pure water at a $pCO_{2(g)}$ of $10^{-3.5}$ bar, i.e. ambient atmospheric conditions, results in a pH of ~8.3 at 25 °C, 1 bar). In the S2 base case simulation, the pH of the cement porewater next to the groundwater boundary did not reach such low values.

5.2. Evolution of backfill hydraulic properties

An assumption made in the base case models was that permeability was not coupled to porosity, thereby promoting alteration due to advective flow through regions clogged with secondary minerals (as it was considered that this may introduce a degree of caution, in that alteration could be promoted). In the S1 'permeability' variant simulation, permeability was coupled to porosity, such that as porosity decreased due to pore clogging, the permeability also decreased. Unsurprisingly, this resulted in a reduction in the predicted rate of cement alteration at the interface with the groundwater boundary condition, leading to pore clogging being slower.

The rate at which porosity was lost in the cement at the groundwater boundary in the simulations depended on the composition of the water. In the S1 base case, pore clogging was complete after 78 years, in contrast it was much slower in the S2 base case, where the water had a relatively lower ionic strength. Interestingly, the rate of clogging was much more rapid than that reported in a previous study [7], but it is noted that the width of cells included in model grids will influence the rate of porosity occlusion [14]. The use of grids with narrower spacing between cells tends to result in pore clogging occurring at a faster rate, as there is a smaller volume available for the growth of secondary solids. The rate of precipitation of secondary solids (one of the uncertainties associated with reactive-transport models in general), will also influence rate of clogging (see subsequent discussion). Therefore, the times at which clogging is complete, should be taken to be approximate, and the potential for variation should be noted.

It was beyond the scope of the study to explicitly model the evolution of backfill cracking/fracturing and the possible extent to which such features may be blocked by secondary mineral precipitation or to consider the potential that there may be for larger advective flow paths to become 'armoured' with alteration products and remain open (although such models have been developed e.g. [22]). However, variant cases were explored to consider the effect of model assumptions related to pore clogging and transport coupling on model outputs. In the base case models, NRVB was assumed to have the same hydraulic conductivity as measured on fresh material. However, in performance assessment calculations, a factor of 10 greater was assumed, given the potential for cracking to occur over time. The S1 'cracked' variant illustrates that widespread, smaller scale cracking could increase hydraulic conductivity, resulting in higher fluxes of reactants into the cement matrix and the potential for faster rates of alteration (and pore clogging) to occur near to the cement-groundwater interface. Alternatively, a smaller number of relatively larger cracks could result in water flow being channelled with the development of essentially stagnant zones in the backfill matrix. Such a scenario was outside the scope of this work but could be considered in future work.

In the 'cracked' and 'permeability coupled' variants, complete pore clogging is predicted to occur relatively quickly (in the order of tens of years) and alteration essentially shuts down. It could be the case in a deep geological disposal facility for radioactive wastes that a very small amount of pore space remains open and that reactions continue, albeit at a slow rate, through largely clogged alteration zones. However, once pore space has largely been blocked, it seems likely that alteration could only proceed at an extremely slow rate. The 'no clogging' variant was produced to explore potential alteration after large volumes of groundwater had reacted with NRVB (noting that excluding all clogging is unrealistic). In this simulation solute transport was decoupled from porosity and mineral precipitation was allowed to continue past the point at which volumes of minerals exceed the volumes of model compartments (i.e. porosity evolution is decoupled from transport). In this case, alteration fronts moved through the cement that are being dominated by products of sulphate attack (such as ettringite and thaumasite). An alteration zone nearer to the groundwater boundary initially consisted of products of magnesium attack (brucite and magnesium-rich silicate minerals) and carbonation (calcite formation).

5.3. Implications for radioactive waste disposal

The implications that cement degradation will have for the performance of a radioactive waste disposal concept will depend on the desired safety function(s) of the cement. In the 2010 UK concept for Intermediate Level Waste (ILW) disposal in a 'higher-strength' crystalline host rock, NRVB is included as a backfill to give alkaline conditions to limit the solubility of some contaminants and to have a high capacity for sorption, thereby providing a 'chemical barrier' to migration. In addition to chemical requirements, physical properties are specified: the compressive strength of NRVB is relatively low (compared to structural concretes) to aid waste retrievability, if required, and the relatively high porosity of NRVB allows uniform chemical conditions to be maintained and facilitates the release of gases generated by the waste. In the reactive transport models, chloride attack and Friedel's salt formation resulted in elevated cement porewater pH values (as high as ~13) and this could in beneficial in terms of longevity of the 'chemical barrier' function of the backfill, where elevated pH was desirable for minimizing radionuclide migration. However, the increase in pH may by relatively short-lived, depending on whether other forms of cement degradation are occurring. It should also be noted that the increase in pH due to Friedel's salt formation would tend to increase the solubility of silicate minerals present in the host rock, but this is only likely to be an issue for enhancing the potential for solute transport if there is lack of secondary mineral precipitation in void spaces (either in the backfill or host rock).

Sulphate attack may occur as cement is leached by groundwater that has significant dissolved sulphate concentrations, such as those close to, or at gypsum saturation. Sulphate attack can lead to strength loss, expansion, cracking and, ultimately, disintegration. Therefore, there may be the possibility of sulphate attack increasing cracking. However, our understanding of crack formation under significant confining pressure in a deep radioactive waste disposal facility, and the amount of healing that may occur due to precipitation of secondary minerals is limited. Cracking could increase the permeability of the backfill and could affect its mechanical properties as could the loss of C-S-H gel due to thaumasite sulphate attack.

For groundwaters that have a relatively low sulphate and chloride concentrations, leaching and carbonation are likely to be the predominant types of cement alteration (carbonation is also likely to arise from CO_2 release from degrading wastes). Although the reduction in cement porewater pH due to leaching and carbonation is not desirable in terms of maintaining a high pH to minimize radionuclide migration, it can result in a degree of pore clogging, thereby reducing solute transport and possibly leading to some degree of crack healing. However, it is not clear from current data what the balance between crack formation and healing (along with clogging of matrix porosity) could be. In addition, the possibility of the formation and subsequent 'armouring' (and lack of closure) of any larger transmissive features is not that clear and could be explored in future work.

5.4. Model uncertainties

A lack of measured dissolution rates for some cement solids and possible secondary minerals also meant that an analogue approach had to be used. The 'alternative kinetics' variant simulation provides some indication of the effect of varying mineral dissolution/precipitation rates and reactive surface areas, and for the relatively short duration of these models (due to pore clogging after tens of years of reaction) the same overall models of alteration were predicted as in the base case simulation. For simulations of many thousands or many tens of thousands of years, assumptions made surrounding reaction kinetics will be more important for predicting rates of cement degradation. However, the difficulties associated with simulating the rates of complex mineral-fluid reactions are common to several materials associated with radioactive waste disposal concepts, not just cement [e.g. 16, 17]. It would therefore seem prudent to consider possible ranges in mineral dissolution/precipitation rates and surface areas in models of specific near-field barrier concepts in future work. Other, probably less significant, sources of uncertainty include errors inherent in the standard molal thermodynamic data used in the modelling. The need to use analogue approaches for mineral dissolution/precipitation kinetics demonstrate a need for continued work to constrain reaction rates, or demonstrate the importance of their variability in reactive transport simulations of cement.

6. Conclusions

1-D reactive-transport models were constructed to simulate a block of cementitious NRVB (1 m thick) that is in contact with two illustrative groundwater compositions with different sulphate and chloride concentrations. The models suggest that different groundwater compositions will result in different cement alteration pathways that have different implications for pH evolution (and therefore the potential behaviour of contaminants released from wastes). The alteration of hydrogarnet to Friedel's salt in the presence of water with higher dissolved chloride concentration resulted in an increase in cement porewater pH up to a value of ~13, which would also potentially increase the potential for alteration of the host rock by hyperalkaline fluids. In contrast, the formation of products associated with reaction with Mg-rich waters would tend to lead to a reduction in pH to ~10 and in a system dominated by calcium carbonate precipitation, pH may fall to ~8 depending on pCO_2. The models also show that thaumasite could potentially form as a product of sulphate attack on NRVB, something that has not been considered in previous work.

The rate at which porosity was lost in the cement matrix at the groundwater boundary in the simulations depended on the composition of the water. However, it should be noted that the spatial resolution of reactive transport model grids will have had some influence on predicted rates of clogging, as will mineral precipitation rates (which at present, are not well-constrained). The rate of pore clogging and implications for evolution of radioactive waste disposal systems is an area that may benefit from further work. The implications that changes to the physical and chemical properties of backfill will have for the performance of a radioactive waste disposal concept, will depend on the desired safety function(s) of the cement.

The uncertainties associated with the data used in reactive transport models (such as growth rates of secondary solids) highlight the potential for future studies to generate data to allow model uncertainties to be reduced and/or their implications to be understood more clearly. Continued work on modelling natural/industrial analogues and longer-term cement experiments is also likely to be useful for testing the predictive capacity of reactive transport models that are used to inform performance assessments of radioactive waste disposal facilities and to further develop modelling capabilities.

Acknowledgements

The authors would like to thank the editorial team and the reviewers. The work presented herein was part of a larger study for RWM Ltd., under a contract with Amec Foster Wheeler (now part of Wood).

References

[1] Radioactive Waste Management Ltd. (RWM), Engineered Barrier System Status Report. NDA Report no. DSSC/452/01, Nuclear Decommissioning Authority, Harwell, UK, 2016.
[2] Swedish Nuclear Fuel and Waste Management Co. (SKB), Safety Analysis SFR 1 Long Term Safety. SKB Report R-08-130, Swedish Nuclear Fuel and Waste Management Co, Stockholm, Sweden, 2008.
[3] P.B. Bamforth, G.M.N. Baston, J.A. Berry, F.P. Glasser, T.G. Heath, C.P. Jackson, D. Savage, S.W. Swanton, Cement Materials for Use as Backfill, Sealing and Structural Materials in Geological Disposal Concepts. A Review of Current Status, SERCO Report SERCO/005125/001 Issue 3, RWMD, Harwell, 2012.
[4] A.W. Harris, M.C. Manning, A.M. Thompson, Testing of models of the dissolution of cements - leaching behaviour of Nirex Reference Vault Backfill, AEA Technology Report, AEAT/ERRA-0316, Nirex Ltd., Harwell, UK, 2001.
[5] G. Purser, A.E. Milodowski, J.F. Harrington, C.A. Rochelle, A. Butcher, D. Wagner, Modification to the flow properties of repository cement as a result of carbonation, Procedia Earth Planet. Sci. 7 (2013) 701–704.
[6] A.E. Milodowski, C.A. Rochelle, G. Purser, Uptake and retardation of cl during cement carbonation, Procedia Earth Planet. Sci. 7 (2013) 594–597.
[7] A.R. Hoch, G.M.M. Baston, F.P. Glasser, F.M.I. Hunter, V. Smith, Modelling evolution in the near field of a cementitious repository, Mineral. Mag. 76 (2012) 3055–3069.
[8] L. De Windt, F. Marsal, E. Tinseau, D. Pellegrini, Reactive transport modeling of geochemical interactions at a concrete/argillite interface, Tournemire site (France), Phys. Chem. Earth 33 (2008) S295–S305.
[9] D. Savage, D. Noy, M. Mihara, Modelling the interaction of bentonite with hyperalkaline fluids, Appl. Geochem. 17 (2002) 207–223.
[10] E.C. Gaucher, P. Blanc, J.-M. Matray, N. Michau, Modeling diffusion of an alkaline plume on a clay barrier, Appl. Geochem. 19 (2004) 1505–1515.
[11] O. Bildstein, L. Trotignon, M. Perronnet, M. Jullien, Modelling iron-clay interactions in deep geological disposal, Phys. Chem. Earth 31 (2006) 618–625.
[12] C. Watson, S. Benbow, D. Savage, Modelling the Interaction of Low pH Cements and Bentonite. Issues Affecting the Geochemical Evolution of Repositories for Radioactive Waste. SKI Report 2007:30, Swedish Nuclear Power Inspectorate, Stockholm, Sweden, 2007.
[13] C. Watson, K. Hane, D. Savage, S. Benbow, J. Cuevas, R. Fernandez, Reaction and diffusion of cementitious water in bentonite: results of 'blind' modelling, Appl. Clay Sci. 45 (2009) 54–69.
[14] N.C.M. Marty, C. Tournassat, A. Burnol, E. Giffault, E.C. Gaucher, Influence of reaction kinetics and mesh refinement on the numerical modelling of concrete/clay interactions, J. Hydrol. 364 (2009) 58–72.
[15] N. Marty, B. Fritz, A. Clément, N. Michau, Modelling the long term alteration of the engineered bentonite barrier in an underground radioactive waste repository, Appl. Clay Sci. 47 (2010) 82–90.
[16] J.C. Wilson, S. Benbow, C. Watson, H. Sasamoto, D. Savage, Fully-coupled reactive transport models of the iron-bentonite interface, Appl. Geochem. 61 (2015) 10–28.
[17] J.C. Wilson, S. Benbow, R. Metcalfe, H. Lueng, Reactive transport modelling of a shale-bentonite interface in a hypersaline system, Appl. Geochem. 76 (2017) 60–73.
[18] D. Savage, J. Liu, Water/clay ratio, clay porosity models and impacts upon clay transformations, Appl. Clay Sci. 116–117 (2015) 16–22.
[19] D. Savage, A review of analogues of alkaline alteration with regard to long-term barrier performance, Mineral. Mag. 75 (2011) 2401–2418.
[20] C. Watson, D. Savage, J. Wilson, S. Benbow, C. Walker, S. Norris, The Tournemire industrial analogue: reactive transport modelling of a cement-clay interface, Clay Miner. 48 (2013) 167–184.
[21] P. Soler, Two-dimensional reactive transport modeling of the alteration of a fractured limestone by hyperalkaline solutions at Maqarin (Jordan), Appl. Geochem. 66 (2016) 162–173.
[22] C. Watson, J. Wilson, D. Savage, S. Benbow, S. Norris, Modelling reactions between alkaline fluids and fractured rock: the Maqarin natural analogue, Appl. Clay Sci. 121–122 (2016) 46–56.
[23] D. Savage, S. Benbow, C. Watson, H. Takase, K. Ono, C. Oda, A. Honda, Natural systems evidence for the alteration of clay under alkaline conditions: an example from Searles Lake California, Appl. Clay Sci. 47 (2010) 72–81.
[24] J.M. Soler, U.K. Mäder, Mineralogical alteration and associated permeability changes induced by a high-pH plume: modeling of a granite core infiltration experiment, Appl. Geochem. 22 (2007) 17–29.
[25] D. Savage, J.M. Soler, K. Yamaguchi, C. Walker, A. Honda, M. Inagaki, C. Watson, J. Wilson, S. Benbow, I. Gaus, J. Rueedi, A comparative study of the modelling of cement hydration and cement-rock laboratory experiments, Appl. Geochem. 26 (2011) 1138–1152.
[26] C. Watson, J. Wilson, D. Savage, Blind Geochemical Modelling of the LCS Experiment. A Detailed Model of the Evolution of the Cement Source. Quintessa Report QRS-1523D-1 v1.0, for RWM Limited, Nuclear Decommissioning Authority, Harwell, UK, 2016.
[27] Nuclear Decommissioning Authority, Generic Disposal Facility Designs. NDA Report

NDA/RWMD/048, Nuclear Decommissioning Authority, Harwell, UK, 2010.
[28] Quintessa, MINARET, Quintessa Ltd., UK, https://www.quintessa.org/software/custom-software/minaret.html, (2017) , Accessed date: 30 October 2017.
[29] Quintessa, QPAC: Quintessa's General-Purpose Modelling Software. Quintessa Report QRS-QPAC-11 Version 1.0. Henley-on-Thames, UK, (2010).
[30] C.E. Watson, D. Savage, J. Wilson, C. Walker, S.J. Benbow, The long-term cement studies project: the UK contribution to model development and testing, Mineral. Mag. 76 (2012) 3445–3455.
[31] D.L. Parkhurst, C.A.J. Appelo, User's guide to PHREEQC (version 2)—a computer program for speciation, batch-reaction, one-dimensional transport, and inverse geochemical calculations, Water-Resources Investigations Report 99-4259, US Department of the Interior, US Geological Survey, Denver, USA, 1999.
[32] P. Aagaard, H.C. Helgeson, Thermodynamic and kinetic constraints on reaction rates among minerals and aqueous solutions. I. Theoretical considerations, Am. J. Sci. 282 (1982) 237–285.
[33] J.L. Palandri, Y.K. Kharaka, A compilation of rate parameters of mineral-water interaction kinetics for application to geochemical modelling, US Geological Survey Open File Report 2004-1068. USA, (2004).
[34] T.R. Holland, W.M. Tearle, A Review of NRVB Mineralogy, SERCO Report SERCO/ERRA-0455, Nirex Ltd., Harwell, UK, 2003.
[35] T. Matschei, B. Lothenbach, F.P. Glasser, Thermodynamic properties of Portland cement hydrates in the system $CaO–Al_2O_3–SiO_2–CaSO_4–CaCO_3–H_2O$, Cem. Concr. Res. 37 (2007) 1379–1410.
[36] K.A. Bond, C.J. Tweed, Groundwater compositions for the Borrowdale Volcanics Group, boreholes 2, 4 and RCF3, Sellafield, evaluated using thermodynamic modelling, Nirex Report NSS/R397, Nirex Ltd., Harwell, UK, 1995.
[37] Nirex, Sellafield geological and hydrogeological investigations: the hydrochemistry of Sellafield, 1997 update, Nirex Science Report, S/97/089, Nirex Ltd., Harwell, UK, 1997.
[38] H.F.W. Taylor, Cement Chemistry, Academic Press, London, UK, 1990.
[39] N.R. Buenfeld, J.B. Newman, The development and stability of surface layers on concrete exposed to sea-water, Cem. Concr. Res. 16 (1986) 721–732.
[40] P.W. Brown, Thaumasite formation and other forms of sulphate attack, Cem. Concr. Compos. 24 (2002) 301–303.
[41] N. Crammond, The occurrence of thaumasite in modern construction – a review, Cem. Concr. Compos. 24 (2002) 393–402.
[42] Thaumasite Expert Group, The Thaumasite Form of Sulphate Attack: Risks, Diagnosis, Remedial Works and Guidance on New Constructions, Department of the Environment, Transport and the Regions (DETR), London, UK, 1999.
[43] D.E. MacPhee, S.J. Barnett, Solid solution properties in the ettringite-thaumasite solid solution series, Cem. Concr. Res. 34 (2004) 1591–1598.
[44] M. Balonis, B. Lothenbach, G. Le Saout, F.P. Glasser, Impact of chloride on the mineralogy of hydrated Portland cement systems, Cem. Concr. Res. 40 (2010) 1009–1022.
[45] D. Savage, C. Walker, R. Arthur, C. Rochelle, C. Oda, H. Takase, Alteration of bentonite by hyperalkaline fluids: a review of the role of secondary minerals, Phys. Chem. Earth 32 (2007) 287–297.
[46] S.J. Chipera, J.A. Apps, Geochemical stability of natural zeolites, in: D.L. Bish, D.W. Ming (Eds.), Natural Zeolites: Occurrence, Properties, Applications, Reviews in Mineralogy and Geochemistry, 45, Mineralogical Society of America, Washington D.C. and the Geochemical Society, St. Louis, Missouri, USA, 2001, pp. 117–162.
[47] R. Arthur, H. Sasamoto, C. Walker, M. Yui, Polymer model of zeolite thermochemical stability, Clay Clay Miner. 59 (2011) 626–639.
[48] M. Santhanam, M.D. Cohen, J. Olek, Mechanism of sulfate attack: a fresh look part I: summary of experimental results, Cem. Concr. Res. 32 (2002) 915–921.
[49] D.R.M. Brew, F.P. Glasser, Synthesis and characterisation of magnesium silicate hydrate gels, Cem. Concr. Res. 35 (2005) 85–98.
[50] C.M. Bethke, Geochemical and Biogeochemical Reaction Modeling, Cambridge University Press, Cambridge, 2008.
[51] T.J. Wolery, EQ3/6 A Software Package for Geochemical Modeling of Aqueous Systems: Package Overview and Installation Guide (Version 7.0), Lawrence Livermore National Laboratory, 2007.
[52] P. Blanc, A. Lassin, P. Piantone, M. Azaroual, N. Jacquemet, A. Fabbri, E.C. Gaucher, Thermoddem: a geochemical database focused on low temperature water/rock interactions and waste materials, Appl. Geochem. 27 (2012) 2107–2116.
[53] L. Duro, M. Grivé, E. Giffaut, ThermoChimie, the ANDRA thermodynamic database, MRS Proc. 1475 (2012).
[54] B. Lothenbach, T. Matschei, G. Moschner, F.P. Glasser, Thermodynamic modelling of the effect of temperature on the hydration and porosity of Portland cement, Cem. Concr. Res. 38 (2008) 1–18.
[55] J.W. Johnson, E.H. Oelkers, H. Helgeson, SUPCRT92: a software package for calculating the standard molal thermodynamic properties of minerals, gases, aqueous species, and reactions for 1–5000 bar and 0–1000 °C, Comput. Geosci. 18 (1992) 899–947.
[56] T. Schmidt, B.L. Lothenbach, M. Romer, K. Scrivener, D. Rentsch, R. Figi, A thermodynamic and experimental study of the conditions of thaumasite formation, Cem. Concr. Res. 38 (2008) 337–349.
[57] S. Baker, S.J. Williams, Measurements of the Solubility of Chromium and the Solubility and Sorption of Molybdenum under Cementitious Repository Conditions. AEA Technology Report AEAT/R/ENV/0531, Nirex Ltd., Harwell, UK, 2001.
[58] H. Helgeson, Thermodynamics of hydrothermal systems at elevated temperatures and pressures, Am. J. Sci. 267 (1969) 729–804.
[59] I. Baur, P. Keller, D. Mavrocordatos, B. Wehrli, C.A. Johnson, Dissolution– precipitation behaviour of ettringite, monosulfate, and calcium silicate hydrate, Cem. Concr. Res. 34 (2004) 341–348.
[60] W.M. Murphy, R.T. Pabalan, J.D. Prikryl, C. Goulet, Reaction kinetics and thermodynamics of aqueous dissolution and growth of analcime and clinoptilolite at 25 °C, Am. J. Sci. 296 (1996) 128–186.
[61] D. Savage, C. Rochelle, Y. Moore, A. Milodowski, K. Bateman, D. Bailey, M. Mihara, Analcime reactions at 25–90 °C in hyperalkaline fluids, Mineral. Mag. 65 (2001) 571–587.
[62] Nuclear Decommissioning Authority, Geological Disposal Generic Post-Closure Safety Assessment, NDA/RWMD/030, Nuclear Decommissioning Authority, Harwell, UK, 2010.
[63] A.W. Harris, A.K. Nickerson, The Physical Properties of the Nirex Reference Vault Backfill, Nirex Report NSS/R335, Nirex Ltd., Harwell, UK, 1997.
[64] B.T. Swift, P.B. Bamforth, A.R. Hoch, C.P. Jackson, D.A. Roberts, G.M.N. Baston, Cracking, flow and chemistry in NRVB, Serco Report Serco/TAS/000505/001 – Issue 3, Nuclear Decommissioning Authority, Harwell, UK, 2010.
[65] A. Honda, K. Masuda, H. Nakanishi, H. Fujita, K. Negishi, Modeling of pH elevation due to the reaction of saline groundwater with hydrated ordinary Portland cement phases, Sci. Basis Nucl. Waste Manag. 1124 (2009) Q10–Q12.